Available online at www.sciencedirect.com
SCIENCE DIRECT
International Journal of Heat and Mass Transfer 49 (2006) 2328–2336
International Journal of HEAT and MASS TRANSFER
www.elsevier.com/locate/ijhmt

New theoretical models of evaporation heat transfer in horizontal microfin tubes

Osamu Makishi [a,*], Hiroshi Honda [b], Y.S. Wang [c]

[a] Department of Mechanical Engineering, University of East Asia, 2-1 Ichinomiyagakuen-cho, Shimonoseki, Yamaguchi 751-8503, Japan
[b] Kyushu University, 337 Kasuya-machi, Kasuya-gun, Fukuoka 811-2307, Japan
[c] State Key Laboratory of Multiphase Flow in Power Engineering, Xi'an Jiatong University, Xi'an 710049, PR China

Received 21 December 2004; received in revised form 18 November 2005
Available online 3 March 2006

Abstract

A stratified flow model and an annular flow model of evaporation heat transfer in horizontal microfin tubes have been proposed. In the stratified flow model, the contributions of thin film evaporation and nucleate boiling in the groove above the stratified liquid level were predicted by a previously reported numerical analysis and a newly developed correlation, respectively. The contributions of nucleate boiling and forced convection in the stratified liquid region were predicted by the new correlation and the Carnavos correlation, respectively. In the annular flow model, the contributions of nucleate boiling and forced convection were predicted by the new correlation and the Carnavos correlation in which the equivalent Reynolds number was introduced, respectively. The flow pattern transition curve between the stratified-wavy flow and the annular flow proposed by Kattan et al. was introduced to predict the heat transfer coefficient in the intermediate region by use of the two theoretical models. The predictions of the heat transfer coefficient compared well with available experimental data for ten tubes and four refrigerants.

Keywords: Evaporation; Refrigerants; Microfin tubes; Stratified flow model; Annular flow model; Flow pattern transition

1. Introduction

Microfin tubes with spiral grooves are widely used for air conditioners and refrigerators as a high performance evaporator tube. A large number of researches have been made on the effects of fin dimensions and fin shape on the heat transfer performance and pressure drop during evaporation in horizontal microfin tubes. On the heat transfer performance, Miyara et al. [1], Murata and Hashizume [2], Kido et al. [3], Koyama et al. [4], Murata [5], Kandlikar and Raykoff [6], Thome et al. [7], Cavallini et al. [8], Yun et al. [9] and Mori et al. [10] have developed correlations of the heat transfer coefficient that are based on the correlations for smooth tubes. Honda and Wang [11] has developed a stratified flow model of evaporation heat transfer in which the effect of surface tension on the vapor–liquid interface profile was taken into account. For the region above the stratified liquid where thin film evaporation is dominant, a numerical analysis using exact boundary conditions was applied. For the stratified liquid region, the correlation proposed by Mori et al. [10] was applied. They compared the predictions of the heat transfer coefficient with available experimental data for four tubes and three refrigerants. The agreement was good in the low mass flux region where the heat flux was also low. In the medium-to-high mass flux region, however, the predictions underpredicted the measured values, with the difference increasing with the mass flux. This was mainly due to the increase in the effect of vapor shear, which resulted in the transition of flow pattern from the stratified flow to the annular flow. Another factor was that the contribution of nucleate boiling in the groove above the stratified liquid level was not taken into account.

* Corresponding author. Tel.: +81 832 57 5046; fax: +81 832 56 9577.
E-mail address: makishi@po.cc.toua-u.ac.jp (O. Makishi).

0017-9310/$ - see front matter © 2006 Elsevier Ltd. All rights reserved.
doi:10.1016/j.ijheatmasstransfer.2005.12.002

Nomenclature

A	cross-sectional area of tube, m^2
A_c	core flow area of tube, $\pi(d-2h)^2/4$, m^2
Bo	boiling number
d	diameter at fin root, m
d_o	outside diameter, m
d_h	hydraulic diameter of tube, m
Fr_0	dimensionless quantity, $G/\sqrt{dg\rho_v(\rho_l-\rho_v)}$
G	refrigerant mass velocity, kg/m^2 s
g	gravitational acceleration, m/s^2
h	fin height, m
h_{lv}	latent heat of vaporization, kJ/kg
M	molar mass
N	number of data
n	number of fins
p	fin pitch, m
P	pressure, Pa
P_c	critical pressure, Pa
P_r	reduced pressure, P/P_c
Pr	Prandtl number
q	heat flux, kW/m^2
r_b	radius of curvature of liquid meniscus, m
r_t	radius of curvature at corner of fin tip, m
$Re_{l,h}$	Reynolds number based on the hydraulic diameter, Gd_h/μ_l
Re_{eq}	equivalent Reynolds number, $Re_{l,h}[1-\chi+(\rho_l/\rho_v)^{1/2}\chi]$
ΔT	wall superheat, K
x, y	curvilinear coordinates, Fig. 3
x_a	connecting point between non-evaporating and evaporating film regions, Fig. 3, m
x_b	connecting point between thin film region and meniscus region, Fig. 3, m
x_c	connecting point between fin flank and fin root tube surface, Fig. 3, m
x_0, x_t	connecting points between straight and round portions of fin, Fig. 3, m
X, Y	Cartesian coordinates, Fig. 3
z	vertical height measured from stratified liquid surface, m
α	heat transfer coefficient, kW/m^2 K
γ	helix angle of groove, deg
δ	liquid film thickness, m
ε_a	surface area enhancement compared to a smooth tube
θ	fin half tip angle, deg
λ	thermal conductivity, kW/m K
μ	dynamic viscosity, Pa s
ρ	density, kg/m^3
σ	surface tension, N/m
φ	angle measured from tube top, rad
φ_s	flooding angle, rad
χ	quality, –
ω	angle, Fig. 1, rad

Subscripts

an	annular model
db	dryout inception point
dc	dryout completion point
ev	evaporation component
fc	forced convection component
l	liquid
m	circumferential average
nb	nucleate boiling component
r	mid-point between adjacent fins at fin root
st	stratified model
v	vapor
1	region 1
2	region 2

In this paper, new theoretical models (i.e., stratified flow model and annular flow model) of evaporation heat transfer in horizontal microfin tubes are proposed. On the basis of available experimental data for evaporation in horizontal microfin tubes, heat transfer correlations for the nucleate boiling component are developed. These correlations are incorporated into the stratified flow model of Honda and Wang [11] to take into account the effect of nucleate boiling explicitly. The annular flow model is based on the equivalent Reynolds number concept and takes into account the effect of nucleate boiling explicitly. The flow pattern transition curve between the stratified-wavy flow and the annular flow proposed by Kattan et al. [12] is introduced to predict the heat transfer coefficient in the intermediate region as a weighted mean of the predictions of the two theoretical models. The predictions of the new theoretical model and previously proposed empirical equations are compared with available experimental data for ten tubes and four refrigerants.

2. Expression for nucleate boiling component

Near the inception point of nucleate boiling, the circumferential average heat transfer coefficient α_m is determined by the contributions of the nucleate boiling component and the forced convection component. If the contributions of these components are assumed to be given by the expression of the form

$$\alpha_m = (\alpha_{nb}^3 + \alpha_{fc}^3)^{1/3} \tag{1}$$

then the heat flux q is given by

$$q = (q_{nb}^3 + q_{fc}^3)^{1/3} \tag{2}$$

Table 1
Tube dimensions

Tube	d_o (mm)	d (mm)	n	h (mm)	p (mm)	x_0 (mm)	r_t (mm)	θ (deg)	γ (deg)	ε_a	l (mm)	l_T (m)	Authors
A	10.0	8.48	60	0.16	0.44	0.027	0.015	19.9	18	1.52	500	6.0	Yu et al.
B	7.0	6.50	50	0.21	0.41	0.019	0.008	19.5	18	1.71	300	3.6	Miyara et al.
C	7.0	6.49	60	0.19	0.34	0.018	0.03	13.1	18	1.78	300	3.6	
D	15.9	14.9	73	0.38	0.64	0.020	0.04	20.8	21.5	1.76	2430	2.43	Del Col et al.
E	7.0	6.46	60	0.15	0.33	0.028[a]	0.02[a]	26.7	18	1.63	300	0.3	Kido et al.
F	7.0	6.45	70	0.21	0.28	0.019[a]	0.02[a]	11.0	11	2.21	300	0.3	
G	7.0	6.49	70	0.21	0.29	0.009[a]	0.02[a]	14.0	17	2.24	300	0.3	
H	7.0	6.48	85	0.16	0.24	0.009[a]	0.02[a]	13.2	9	2.07	300	0.3	
I	7.0	6.50	85	0.16	0.24	0.009[a]	0.02[a]	13.4	17	2.13	300	0.3	
J	7.0	6.44	85	0.21	0.23	0.013[a]	0.02[a]	9.7	7	2.49	300	0.3	

[a] Estimated value.

where q_{nb} is the nucleate boiling component and q_{fc} is the forced convection component. It is assumed that α_{fc} is given by the correlation for the microfin tubes proposed by Carnavos [13] as follows:

$$\alpha_{fc} = 0.023\frac{\lambda_l}{d_h}Re_{l,h}^{0.8}Pr_l^{0.4}\left(\frac{A}{A_c}\right)^{0.1}\varepsilon_a^{0.5}\sec^3\gamma \tag{3}$$

where d_h is the hydraulic diameter, $Re_{l,h} = Gd_h/\mu_l$, G is the mass velocity, A is the cross-sectional area of tube, A_c is the core flow area, ε_a is the surface area enhancement compared to a smooth tube, and γ is the helix angle of groove. Thus, the values of α_{nb} and q_{nb} at $\chi = 0$ are obtained by substituting the values of α_m and q at $\chi = 0$ that are obtained by the interpolation of the curves of α_m versus χ and q versus χ into Eqs. (1)–(3).

In the present paper, the experimental data of Kido et al. [3], Yu et al. [14], Miyara et al. [15] and Del Col et al. [16], where the dimensions of the microfin are clearly described or the picture of fin cross-section are available, are adopted to develop the correlation for the nucleate boiling component. Table 1 shows the tube and fin dimensions, and Table 2 shows the experimental conditions. In Table 1, l is the length of a subsection and l_T is the overall length of the test section. In the data analysis, care must be taken to the accuracy of the measured α_m value. Since the value of average wall superheat ΔT_m is generally small, the accuracy of α_m depends largely on the accuracy of measured wall temperature, Kido et al. [3], Yu et al. [14] and Miyara et al. [15] measured the local wall temperatures at the top, bottom and both sides at the mid-point of each subsection by using thermocouples embedded in the tube outer surface. The diameter of thermocouple wire was 0.3 mm for Kido et al. [3], and 0.1 mm for Yu et al. [14] and Miyara et al. [15]. Del Col et al. [16] obtained α_m from the measured overall heat transfer data by using the heat transfer correlation for the heating water side that was obtained by the Wilson plot method. They also performed pool boiling tests of a flat microfin surface obtained by flattening a piece of the round microfin tube. In this case, the surface temperature was estimated by extrapolating the measured local temperatures in the copper block on which the test surface was soldered. The accuracy of the measured α_m value decreases as ΔT_m decreases. In the present paper, only the experimental data satisfying the condition of $\Delta T_m > 0.7$ K were adopted.

Fig. 1 shows the relationship between α_{nb} and q_{nb} for nine tubes and four refrigerants read from the experimental data of Kido et al. [3], Yu et al. [14] and Miyara et al. [15]. The data are plotted using the parameters of the Cooper

Table 2
Experimental conditions

Tube	Refrigerant	T_{sat} (°C)	G (kg/m^{2}s)	Heating condition
A	R22	8.7–30.9	115–394	Water, c.f. and p.f.[a]
	R134a	18.9–30.9	209–356	
	R123	55.9–59.1	113–309	
B	R410A	10.0–10.3	98–296	Water, c.f.
C	R410A	9.8–10.6	99–299	
D	R22	22	205, 255	
E	R22	−0.5	86–345	Condensation of R114
F	R22	−0.5	173	
G	R22	−0.5	173	
H	R22	−0.5	86, 173	
I	R22	−0.5	86, 173	
J	R22	−0.5	173	

[a] c.f.: counter flow, p.f.: parallel flow.

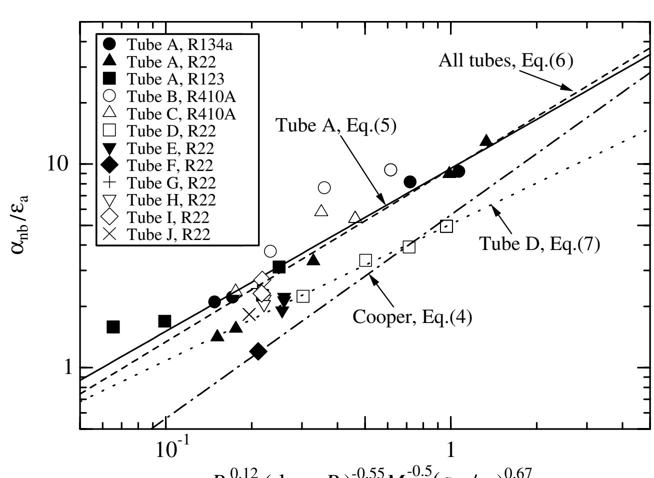

Fig. 1. Relation between α_{nb} and q_{nb} plotted on the coordinates of Cooper correlation.

[17] correlation for pool boiling as the coordinates. In Fig. 1, the pool boiling data obtained by Del Col et al. [16] are also plotted. The dashed line in the figure shows the Cooper [17] correlation for the surface roughness of 1 μm

$$\alpha_{nb} = 5.63\varepsilon_a P_r^{0.12}(-\log_{10}P_r)^{-0.55}M^{0.5}(q_{nb}/\varepsilon_a)^{0.67} \tag{4}$$

where P_r is the reduced pressure, M is the molar mass, and the units of α_{nb} and q_{nb} are kW/m^2 K and kW/m^2, respectively. The experimental data for microfin tubes are considerably scattered and are generally higher than Eq. (4). This is probably due to the difference in the surface roughness among the test tubes. It is also seen that the experimental data for evaporation of R22, R134a and R123 in tube A are correlated fairly well by a straight line. This indicates that the effects of physical properties are expressed fairly well by using the parameter of the Cooper correlation. The solid line in Fig. 1 shows the correlation for tube A:

$$\alpha_{nb} = 9.52\varepsilon_a\{P_r^{0.12}(-\log_{10}P_r)^{-0.55}M^{0.5}(q_{nb}/\varepsilon_a)^{0.67}\}^{0.8} \tag{5}$$

The numbers of data points for tubes B, C, E–J are limited and it is impossible to determine the correlations for these tubes. If we assume the functional form of Eq. (5), the proportionality constants for tubes B, C, E–J are determined to be 14.0, 11.0, 6.0, 4.2, 8.5, 7.1, 8.5 and 7.1, respectively. The broken line in Fig. 1 shows the average correlation for all tubes excepting tube D determined by the least square approximation:

$$\alpha_{nb} = 9.48\varepsilon_a\{P_r^{0.12}(-\log_{10}P_r)^{-0.55}M^{0.5}(q_{nb}/\varepsilon_a)^{0.67}\}^{0.85} \tag{6}$$

and the dotted line shows the correlation for pool boiling on tube D:

$$\alpha_{nb} = 5.07\varepsilon_a\{P_r^{0.12}(-\log_{10}P_r)^{-0.55}M^{0.5}(q_{nb}/\varepsilon_a)^{0.67}\}^{0.68} \tag{7}$$

The slopes of Eqs. (5) and (6) are smaller than that of the Cooper correlation (4), and the slope of Eq. (7) is even smaller.

3. Theoretical model

3.1. Stratified flow model

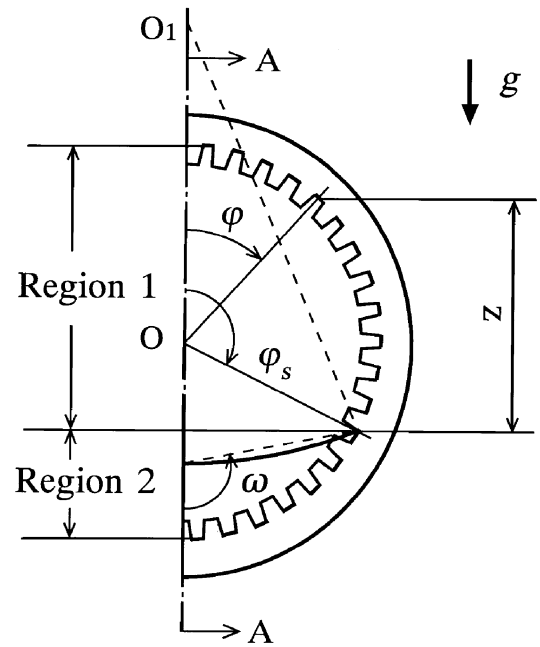

Fig. 2. Physical model of stratified flow in a horizontal microfin tube.

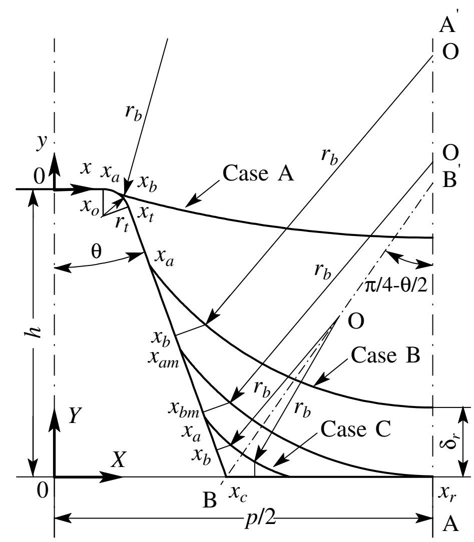

Fig. 3. Liquid film profiles in fin cross-section of region 1.

Fig. 2 shows the physical model of stratified flow in a horizontal microfin tube. The angle φ is measured from the top of tube and φ_s is the flooding angle below which the tube is filled with stratified liquid. The coordinate z is measured vertically upward from the liquid vapor interface at $\varphi = \varphi_s$. The tube surfaces at the angular portions $0 \leqslant \varphi \leqslant \varphi_s$ and $\varphi_s \leqslant \varphi \leqslant \pi$ are denoted as region 1 and region 2, respectively. The profile of stratified liquid is assumed by a circular arc centered at O_1. The void fraction and the angle ω in Fig. 2 are determined by the method described in Honda and Wang [11].

Fig. 3 shows the liquid film profile of a well wetting liquid in the fin cross-section in region 1. The fin profile is approximated by a trapezoid with a round corner at the fin tip. The fin height, fin pitch, fin half-tip angle and the radius of curvature at the corner of fin tip are denoted as h, p, θ and r_t, respectively. The coordinate x is measured along the fin surface from the center of fin tip and y is measured vertically outward from the fin surface. The X and Y are the Cartesian coordinates measured horizontally and vertically upward from the mid-point at fin root, respectively. The connecting points between the straight and round portions at the fin tip are x_0 and x_t. The x coordinate at the fin root is x_c, and that at the mid-point between adjacent fins is x_r. Liquid is pulled up above the level of stratified liquid by the capillary effect and retained in the groove between adjacent fins. The radius of curvature of the liquid meniscus r_b is assumed to be determined by the static force balance between the surface tension and gravity forces as follows:

$$\frac{\sigma}{r_b} = (\rho_l - \rho_v)gz = \frac{(\rho_l - \rho_v)gd}{2}(\cos\varphi - \cos\varphi_s) \tag{8}$$

The liquid film in the fin cross-section is divided into three regions: a non-evaporating film region, a thin film region with a high evaporation rate and a meniscus region with a relatively low evaporation rate. The connecting point between the non-evaporating film region and the evaporating film region is denoted as x_a, and the connecting point between the thin film region and the meniscus region is denoted as x_b. The liquid film profile is divided into three cases; Case A, Case B and Case C, depending on the position of x_a. In Case A for $x_0 < x_a < x_t$ and Case B for $x_t < x_a < x_{am}$, the liquid film profile is symmetrical with respect to the line A–A' ($X = p/2$), where x_{am} denotes the position of x_a at which the liquid film thickness at $x = x_r$, δ_r, is equal to zero. In Case C for $x_{am} < x_a < x_r$, the liquid film profile is symmetrical with respect to the line B–B'. In this case the non-evaporating film region and the thin film region exist on both the fin flank and the fin root tube surface. Numerical calculation of the liquid film profile was conducted for about 20 values of x_a that changed in between x_0 and x_c. The value of x_{am} is determined empirically on the basis of the numerical calculation of liquid film profile for different x_a. The details of the calculation procedure is described in Honda and Wang [11].

The heat transfer coefficient for region 1, α_1, consists of the evaporation component α_{ev1} and the nucleate boiling component α_{nb1}, where α_{ev1} is determined by the thin film evaporation model of Honda and Wang [11] and α_{nb1} is obtained by multiplying the value of α_{nb} given by Eqs. (5)–(7), etc. with the area ratio of the thick film region in the groove to the total surface area of region 1. Thus the expression for α_1 is written as

$$\alpha_1 = \alpha_{ev1} + \alpha_{nb1} \tag{9}$$

The value of α_{nb1} is obtained from

$$\alpha_{nb1} = \alpha_{nb}\left[2\int_0^{\varphi_{bm}}(x_c - x_b)\mathrm{d}\varphi + \int_{\varphi_{bm}}^{\varphi_s}(x_r - x_b)\mathrm{d}\varphi\right]\Big/ x_r\varphi_s \quad \text{for } r_{b0} < r_{bm} \tag{10-1}$$

and

$$\alpha_{nb1} = \alpha_{nb}\int_0^{\varphi_s}(x_r - x_b)\mathrm{d}\varphi / x_r\varphi_s \quad \text{for } r_{b0} \geqslant r_{bm} \tag{10-2}$$

where r_{b0} is the value of r_b obtained by substituting $\varphi = 0$ into Eq. (8), r_{bm} is the value of r_b that corresponds to $x_b = x_{bm}$, and φ_{bm} is the value of φ that corresponds to $x_b = x_{bm}$.

The heat transfer coefficient for region 2, α_2, is obtained by the following equation:

$$\alpha_2 = (\alpha_{nb2}^3 + \alpha_{fc2}^3)^{1/3} \tag{11}$$

where α_{nb2} is the nucleate boiling component obtained from Eqs. (5)–(7) and α_{fc2} is the forced convection component obtained by applying Eq. (3) to the stratified liquid region. The definition of d_h for the stratified liquid region is given in Honda and Wang [11]. The circumferential average heat transfer coefficient α_m is obtained by the following equation for the uniform heat flux condition:

$$\alpha_m = \frac{\pi q}{\varphi_s\Delta T_1 + (\pi - \varphi_s)\Delta T_2} = \left\{\frac{\varphi_s}{\pi}\frac{1}{\alpha_1} + \left(1 - \frac{\varphi_s}{\pi}\right)\frac{1}{\alpha_2}\right\}^{-1} \tag{12}$$

where $\Delta T_1 = q/\alpha_1$, $\Delta T_2 = q/\alpha_2$.

3.2. Annular flow model

In the annular flow model, the effect of vapor shear force on the forced convection component α_{fc} is assumed to be expressed by substituting the equivalent Reynolds number $Re_{eq} = (Gd_h/\mu_l)\,[1 - \chi + (\rho_l/\rho_v)^{1/2}\chi]$ into $Re_{l,h}$ of Eq. (3) as follows:

$$\alpha_{fc} = 0.023\frac{\lambda_l}{d_h}Re_{eq}^{0.8}Pr_l^{0.4}\left(\frac{A}{A_c}\right)^{0.1}\varepsilon_a^{0.5}\sec^3\gamma \tag{13}$$

The nucleate boiling component α_{nb} is given by Eqs. (5)–(7). Then, α_m is assumed to be given by the following equation:

$$\alpha_m = (\alpha_{fc}^3 + \alpha_{nb}^3)^{1/3} \tag{14}$$

4. Comparison of theoretical predictions with experimental data

The predictions of α_m by the two theoretical models were compared with the measured heat transfer coefficients for ten tubes and four refrigerants shown Tables 1 and 2. In the data reduction, the average quality of a subsection or a test section was used as the experimental data. The quality change in each subsection was less than 0.21, 0.19 and 0.23 for tubes A, B and C, respectively, and the quality change in the test section was less than 0.3 for tube D and less than 0.11 for tubes E–J. As described in the previous section, the magnitude of nucleate boiling component α_{nb} was considerably different depending on the test tubes. This was probably due to the difference in the surface roughness. However, no information was available about the surface roughness and it was impossible to derive a general correlation for α_{nb} taking account of the surface roughness. In the following discussion, two cases are examined for the expression of α_{nb}. In case 1, the expression of α_{nb} for each tube described in the previous section was used. In case 2, the average correlation given by Eq. (6) was used for all tubes.

Fig. 4(a)–(d) compare the predictions of the stratified flow model and the annular flow model with the experimental data for the evaporation of R22 in tube A. In the theoretical models, α_{nb} was predicted by use of Eq. (5). The value of the dimensionless number $Fr_0 =$

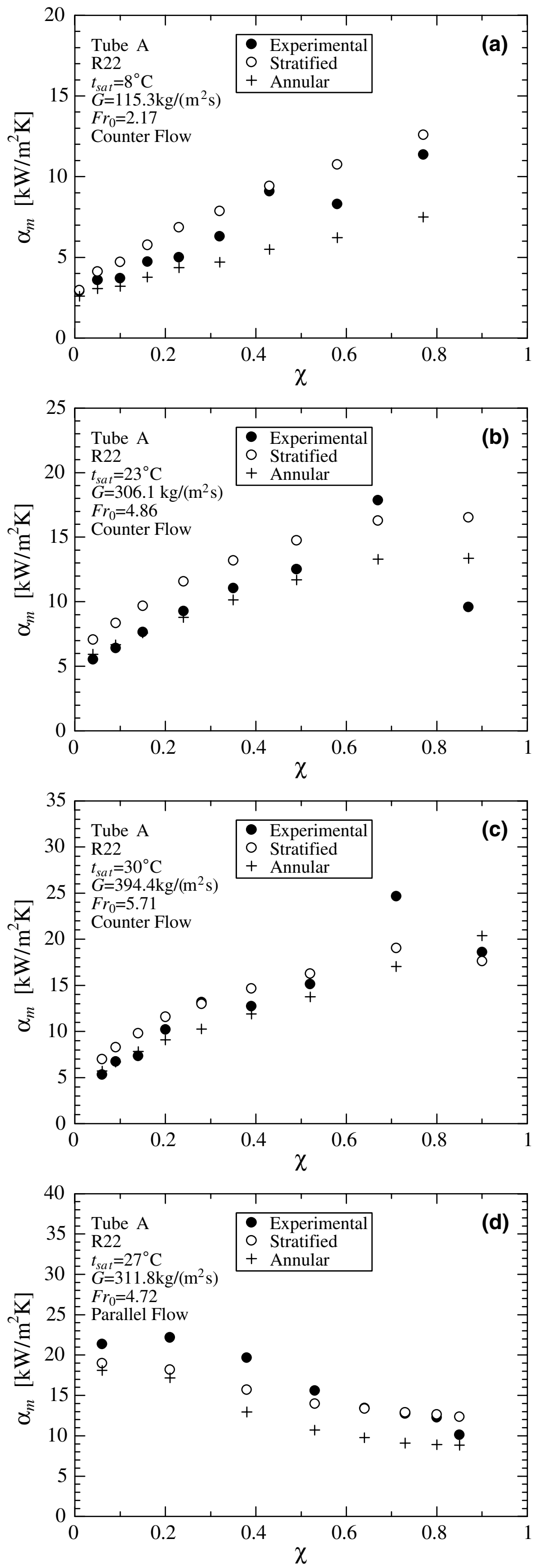

Fig. 4. Comparison of measured and predicted $\alpha_{\rm m}$ values.

$G/\sqrt{dg\rho_{\rm v}(\rho_{\rm l}-\rho_{\rm v})}$, which is a measure of the flow pattern transition, is also shown in the figures. Fig. 4(a)–(c) show the results for the counter flow of refrigerant and heating water in the increasing order of G. The stratified flow model gives a higher $\alpha_{\rm m}$ than the annular flow model and the difference between the two predictions decreases with the increase in G. The experimental data is located in the middle of the two predictions. Fig. 4(d) shows the result for the parallel flow of refrigerant and heating water at $G = 312$ kg/m^2 s. In this case the distribution of $\alpha_{\rm m}$ is considerably different from those for the counter flow. This is due to the difference in the distribution of $\alpha_{\rm nb}$ between the two cases. In the case of counter flow, $\Delta T_{\rm m}$ takes a small value near the inlet of the refrigerant (i.e., at small χ) and increases with increasing χ. Since $\alpha_{\rm nb}$ is proportional to the power of $\Delta T_{\rm m}$, $\alpha_{\rm nb}$ also increases with increasing χ. In the case of parallel flow, on the other hand, $\Delta T_{\rm m}$ takes a large value near the inlet of the refrigerant and decreases with increasing χ. Consequently, $\alpha_{\rm nb}$ takes a large value at small χ and decreases with increasing χ. It is seen in Fig. 4(d) that the experimental data are larger than the predictions of the two theoretical models. This indicates that the correlation for $\alpha_{\rm nb}$ is not satisfactory at large $\Delta T_{\rm m}$. As described above, $\alpha_{\rm m}$ is closely related to the flow pattern in the tube. Fig. 5(a)–(d), respectively, show the mass velocity at the transition between the stratified-wavy flow and the annular flow, $G_{\rm wavy}$, corresponding to Fig. 4(a)–(d) that are obtained from the flow pattern map proposed by Kattan et al. [12]. Since the Kattan et al. [12] map was obtained for evaporation in smooth tubes, it was modified to the case of microfin tubes as follows:

$$G_{\rm wavy} = \left\{\frac{16(A_{\rm v}/d^2)^3 gd\rho_{\rm l}\rho_{\rm v}}{\pi^2\chi^2(S_{\rm i}/d)}\right\}^{0.5} \times \left\{\frac{\pi^2}{25(h_{\rm l}/d)^2}(1-\chi)^{F_1}\left(\frac{\sigma}{gd^2\rho_{\rm l}}\right)^{F_2}+1\right\}^{0.5} + 50 \tag{15}$$

where $A_{\rm v}$ is the cross-sectional area of the vapor space, $S_{\rm i}$ is the perimeter length of the liquid–vapor interface, $h_{\rm l}$ is the height of the liquid–vapor interface measured from the tube bottom, $F_1 = 646.0(q/q_{\rm c})^2 + 64.8(q/q_{\rm c})$, $F_2 = 18.8(q/q_{\rm c}) + 1.023$ and $q_{\rm c} = 0.131\rho_{\rm v}^{1/2}h_{\rm lv}\{g(\rho_{\rm l}-\rho_{\rm v})\sigma\}^{1/4}$. The values of $A_{\rm v}$, $S_{\rm i}$ and $h_{\rm l}$ were determined by the method described in Honda and Wang [11]. In Fig. 5, where $G_{\rm wavy}$ is plotted as a function of χ, the measured mass velocity G is also plotted. It is seen that $G_{\rm wavy}$ is larger than G in Fig. 5(a), whereas G is larger than $G_{\rm wavy}$ in Fig. 5(b)–(d). Comparison of the counter flow cases in Figs. 4 and 5 reveals that the measured $\alpha_{\rm m}$ is close to the prediction of the stratified flow model when $G_{\rm wavy} \geqslant G$ and it is close to the prediction of the annular flow model when $G > G_{\rm wavy}$. Considering the above results, we propose a general prediction equation for $\alpha_{\rm m}$ of the form

$$\alpha_{\rm m} = (1-a)\alpha_{\rm m,st} + a\alpha_{\rm m,an} \tag{16}$$

where $a = 1/[1 + (G_{\rm wavy}/G)^3]$, and $\alpha_{\rm m,st}$ and $\alpha_{\rm m,an}$ denote the predictions of the stratified flow model and the annular flow model, respectively.

Fig. 6(a)–(d), respectively, compare the predictions of Eq. (16) and previously proposed six correlations with

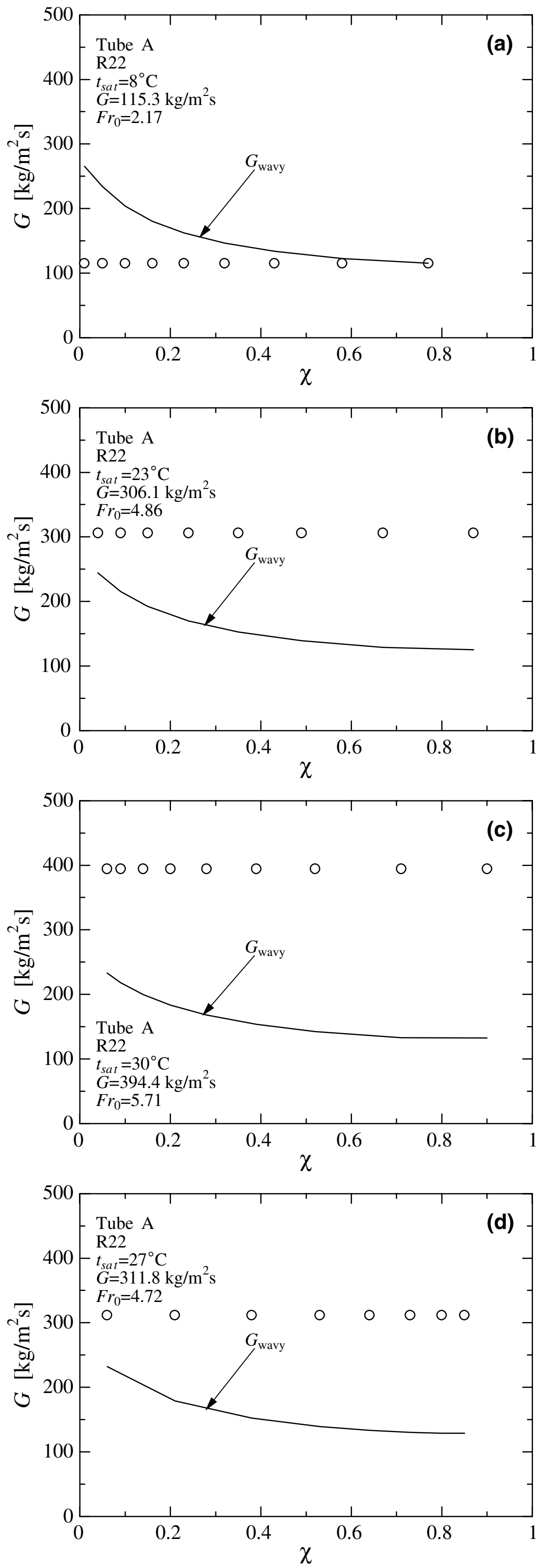

Fig. 5. Variation of G_{wavy} with χ.

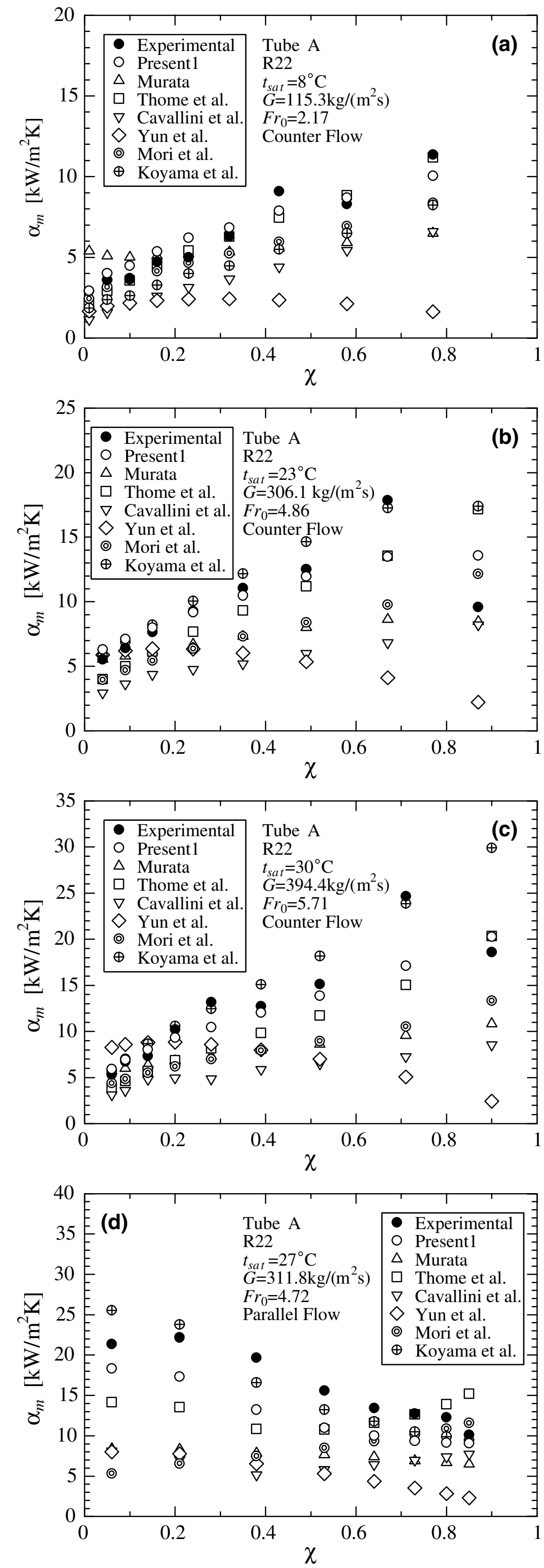

Fig. 6. Comparison of measured and predicted α_m values.

the experimental data shown in Fig. 4(a)–(d). It is seen that the correlation of Yun et al. [9] gives predictions that are generally lower than the experimental data. It is also seen that the difference among the predictions is most significant for the case of parallel flow shown in Fig. 6(d).

Table 3 summarizes the results of comparison between the predictions of the present theoretical model and the previously proposed six correlations with available experimental data for 10 tubes and four refrigerants. For the present theoretical model, the results are presented for

Table 3
Error analysis

Tube	Refrigerant	N	Murata		Koyama et al.		Thome et al.		Cavallini		Yun et al.		Mori et al.		Present 1		Present 2	
			am	rms	am	rms	am	rms	am	rms	am	rms	am	rms	am	rms	am	rms
A	R22	37	−28.2	42.7	−7.5	19.8	−18.4	23.4	−52.0	53.0	−48.1	58.3	−34.2	39.0	−7.9	18.1	−12.5	18.8
A	R134a	31	−30.3	36.5	6.5	23.1	−6.2	28.2	−52.9	55.0	−40.9	49.2	−28.6	36.6	−10.9	19.3	−15.2	21.4
A	R123	28	12.5	28.5	−5.1	21.7	41.8	53.0	−39.5	42.4	−15.7	35.6	16.4	31.7	5.7	16.3	−0.8	14.1
B	R410A	22	−47.9	48.5	−19.4	30.3	−26.8	31.3	−46.3	48.2	−67.3	68.2	−31.1	33.5	21.1	26.8	−19.6	22.9
C	R410A	24	−36.3	41.1	−11.6	22.6	−17.0	21.0	−17.7	25.3	−59.3	61.9	−8.1	20.5	14.7	22.3	−5.0	13.9
D	R22	18	−19.2	19.8	23.9	26.7	16.7	17.9	−38.7	39.0	−43.7	46.2	−26.1	26.3	−18.8	19.6	12.6	17.2
E	R22	25	31.7	41.0	28.5	38.9	104.3	111.5	37.6	39.3	−41.0	50.8	123.0	134.1	28.7	38.3	50.4	55.7
F	R22	8	7.0	29.5	−9.3	19.8	49.9	50.3	95.2	95.6	−57.7	60.7	156.0	157.0	−15.9	16.4	15.7	32.8
G	R22	6	−27.1	29.8	−40.8	41.7	4.5	7.6	11.3	16.7	−69.4	69.9	49.2	50.0	−22.5	26.1	−21.8	25.9
H	R22	14	−18.4	25.0	−30.6	32.5	0.6	15.1	29.8	35.8	−68.5	69.4	49.9	62.1	−11.9	18.1	2.3	19.3
I	R22	15	−25.1	30.7	−35.4	37.2	11.6	31.8	30.8	43.7	−71.5	72.4	47.1	67.2	−6.2	11.9	−5.5	11.9
J	R22	6	−12.5	19.3	−29.1	30.7	5.0	6.7	82.2	84.0	−63.3	64.1	125.5	126.0	−15.0	19.3	−2.6	18.1
All data		234	−16.9	36.4	−5.3	27.9	12.1	46.8	− 15.7	48.2	−49.1	57.1	16.0	67.0	0.4	22.4	−0.4	25.7

am: arithmetic mean value, rms: root mean square value.

two cases. The first one (Present 1) is the case where α_{nb} is calculated by using the correlation for each tube. The second one (Present 2) is the case where α_{nb} is calculated by using Eq. (6) for all tubes. The performance of all models and correlations were estimated in terms of the arithmetic mean error, am, and the root-mean-square error, rms, defined as follows:

$$\mathrm{am} = \frac{1}{N}\sum \frac{\alpha_{m,pre} - \alpha_{m,exp}}{\alpha_{m,exp}} \times 100\% \tag{17}$$

$$\mathrm{rms} = \sqrt{\frac{1}{N}\sum \left(\frac{\alpha_{m,pre} - \alpha_{m,exp}}{\alpha_{m,exp}}\right)^2} \times 100\% \tag{18}$$

The experimental data in the range of $\chi > 0.8$ were excluded from the analysis because they were supposed to be affected by the dryout of the tube surface. Comparison of the results reveals that the rms error for all data decreases in the order of Present 1 (22.4%), Present 2 (25.7%), Koyama [4] (27.9%) and so on. Since Present 1 is based on the correlation of α_{nb} for each tube which is not applicable to the other tubes, Present 2 is considered to be the best practical method for predicting α_m.

An attempt was made to take into account the effect of dryout in the heat transfer model by use of the correlation for the dryout inception condition proposed by Yoshida et al. [18]. Their correlation was based on the experimental data for uniform heat flux and it was not directly applicable to the cases of variable heat flux discussed in the present paper. Thus an interpolation procedure was adopted to estimate the dryout inception quality χ_{db} and the heat transfer coefficient at $\chi = \chi_{db}$. For the local flow condition at each measurement point along the tube, the dryout inception quality $\chi_{db,i}$ $(i = 1,2,\ldots)$ corresponding to the local heat flux q_i was calculated by use of the Yoshida et al. [18] correlation. Then it was compared with the experimental data χ_i. If $\chi_{db,i} \leqslant \chi_i$ and $\chi_{db,i+1} > \chi_{i+1}$ (or vise versa) were satisfied by two successive measurement points along the tube, the local quality at which $\chi_i = \chi_{db}$ was satisfied was obtained by the following equation:

$$\chi_{db} = \frac{\chi_{db,i}\chi_{i+1} - \chi_{db,i+1}\chi_i}{\chi_{i+1} - \chi_i - \chi_{db,i+1} + \chi_{db,i}} \tag{19}$$

Then the heat transfer coefficient at $\chi = \chi_{db}$ was obtained from

$$\alpha_{db} = \frac{(\alpha_{i+1} - \alpha_i)\chi_{db} - \alpha_{i+1}\chi_i + \alpha_i\chi_{i+1}}{\chi_{i+1} - \chi_i} \tag{20}$$

The dryout completion quality was assumed to be unity. Then, for the region of $\chi_{db} < \chi_i < 1$, the heat transfer coefficient at $\chi = \chi_i$ was obtained from

$$\alpha_{m,i} = \frac{\alpha_{db}\chi_{dc} - \alpha_{dc}\chi_{db}}{\chi_{dc} - \chi_{db}} - \frac{\alpha_{db} - \alpha_{dc}}{\chi_{dc} - \chi_{db}}\chi_i \tag{21}$$

where α_{dc} is the heat transfer coefficient at $\chi = 1$ which was obtained by substituting the physical properties of vapor into Eq. (13). The rms errors for all data were 23.4% and 26.7% for the modified Present 1 and Present 2 methods in which the above correction was incorporated, respectively. These values were a little larger than the predictions of the original Present 1 and Present 2 methods.

5. Conclusions

The contribution of nucleate boiling during evaporation in horizontal microfin tubes was examined for available experimental data for ten tubes and four refrigerants. The correlation of the nucleate boiling component for each tube and an average correlation for all tubes were developed using the parameters of the Cooper [17] correlation for pool boiling. A stratified model and an annular flow model of evaporation heat transfer in horizontal microfin tubes in which the above correlations were incorporated were proposed. A good agreement with available experimental data was obtained by the weighted average of the predictions of the two theoretical models taking account of the flow pattern transition curve between the stratified-wavy flow and the annular flow proposed by Kattan et al. [12]. The rms error of the prediction for all data was 22.4% and 25.7% for the cases in which the correlation of the nucleate boiling component for each tube was adopted and the average correlation for all tubes was adopted, respectively. The agreement was better than the predictions of previously proposed six correlations.

References

[1] A. Miyara, H. Takamatsu, K. Koyama, K. Yonemoto, T. Fujii, Forced convective boiling of nonazeotropic refrigerant mixture of R22 and R114 inside a horizontal tube, Trans. Jpn. Soc. Mech. Eng. Ser. B 54 (505) (1988) 2523–2528 (in Japanese).

[2] K. Murata, K. Hashizume, Forced convective boiling of nonazeotropic refrigerant mixtures inside tubes, Trans. Am. Soc. Mech. Eng. J. Heat Transfer 115 (1993) 680–689.

[3] K. Kido, M. Taniguchi, T. Taira, H. Uehara, Evaporation heat transfer and pressure drop of HCFC22 inside an internally grooved horizontal tube, Trans. Jpn. Assoc. Refrig. 11 (2) (1994) 131–142.

[4] S. Koyama, J. Yu, S. Momoki, T. Fujii, H. Honda, Forced convective flow boiling heat transfer of pure refrigerants inside a horizontal microfin tube, in: Proceedings of Engineering Foundation Conference on Convective Flow Boiling, Banff, Canada, Taylor and Francis, 1995, pp. 137–142.

[5] K. Murata, A correlation for forced convective boiling heat transfer of binary refrigerant mixtures: 2nd report, a spirally grooved tube, Trans. Jpn. Soc. Mech. Eng. Ser. B 62 (599) (1996) 2723–2728 (in Japanese).

[6] S.G. Kandlikar, T. Raykoff, Predicting flow boiling heat transfer of refrigerants in micro-fin tubes, J. Enhanc. Heat Transfer 4 (1997) 257–268.

[7] J.R. Thome, N. Kattan, T. Favrat, Evaporation in micro-fin tubes: a generalized prediction model, In: Proceedings of Convective Flow and Pool Boiling Conference, Kloster, Irsee, 1997, paper VII-4.

[8] A. Cavallini, D. Del Col, L. Doretti, G.A. Longo, L. Rosetto, Refrigerant vaporization inside enhanced tubes: a heat transfer model, In: Proceedings of Eurotherm Seminar 62, Grenoble, France, 1998, pp. 222–231.

[9] R. Yun, Y. Kim, K. Seo, H.Y. Kim, A generalized correlation for evaporation heat transfer of refrigerants in micro-fin tubes, Int. J. Heat Mass Transfer 45 (2002) 2003–2010.

[10] H. Mori, S. Yoshida, S. Koyama, A. Miyara, S. Momoki, Prediction of heat transfer coefficients for refrigerants flowing in horizontal spirally grooved evaporator tubes, In: Proceedings of 2002 Japan Society of Refrigerating and Air Conditioning Engineers Annual Conference, Okayama, Japan, 2002, pp. 547–550 (in Japanese).

[11] H. Honda, Y.S. Wang, Theoretical study of evaporation heat transfer in horizontal microfin tubes: stratified flow model, Int. J. Heat Mass Transfer 70 (2004) 3971–3983.

[12] N. Kattan, J.R. Thome, D. Favrat, Flow boiling in horizontal tubes: Part 1—Development of a diabatic two-phase flow pattern map, Trans. Am. Soc. Mech. Eng. J. Heat Transfer 120 (1998) 140–147.

[13] T.C. Carnavos, Heat transfer performance of internally finned tubes in turbulent flow, Heat Transfer Eng. 1 (1980) 32–37.

[14] J. Yu, S. Koyama, S. Momoki, Experimental study of flow boiling heat transfer in a horizontal microfin tube, Reports of the Institute of Advanced Material Study Kyushu University 9, 1995, pp. 27–42.

[15] A. Miyara, Y. Otsubo, S. Ohtsuka, Evaporation heat transfer of R410A in herringbone micro-fin tubes, In: Proceedings IIR Conference, Thermophysical Properties and Transfer Processes of New Refrigerants, Paderborn, Germany, 2001, pp. 314–319 (also private communication).

[16] D. Del Col, R.L. Webb, R. Narayanamurthy, Heat Transfer mechanisms for condensation and vaporization inside a microfin tube, J. Enhanc. Heat Transfer 9 (2002) 25–37.

[17] M.G. Cooper, Saturation nucleate pool boiling: a simple correlation, Inst. Chem. Eng. Symp. Ser. 86 (1984) 786–793.

[18] S. Yoshida, H. Mori, Y. Kakimoto, K. Ohishi, Dryout quality for refrigerants flowing in horizontal evaporator tubes, Trans. Jpn. Soc. Refrig. Air Condition. Eng. 17 (4) (2000) 511–520 (in Japanese).